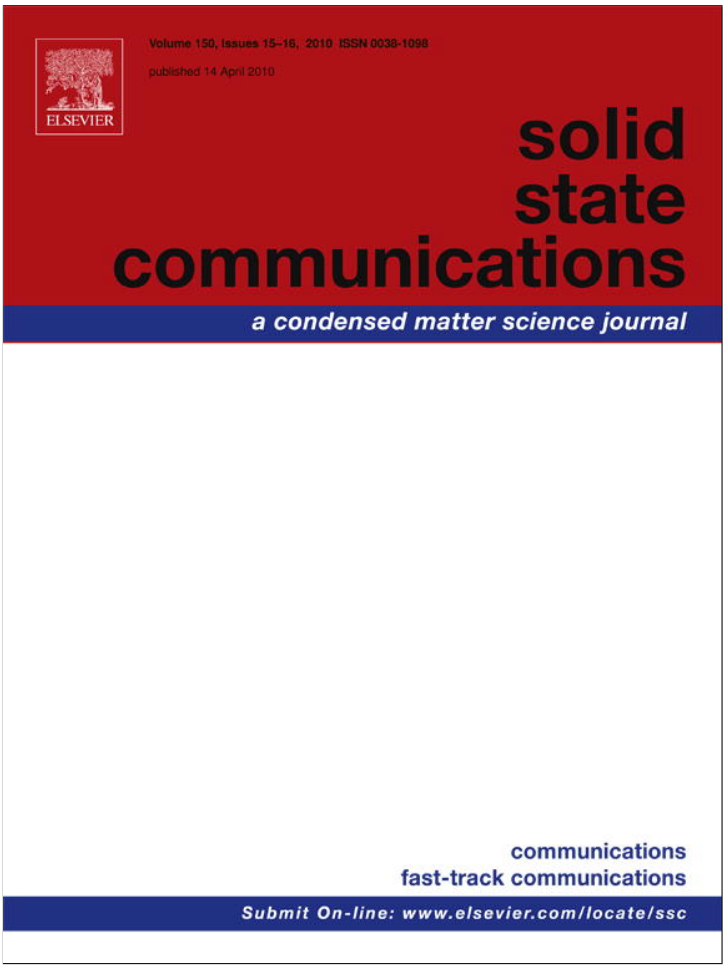

Solid State Communications 150 (2010) 707–710

Contents lists available at ScienceDirect

Solid State Communications

journal homepage: www.elsevier.com/locate/ssc

Interband optical transitions of an InAs/InGaAs dots-in-a-well structure

Rui Chen [a], H.Y. Liu [b], H.D. Sun [a,*]

[a] Division of Physics and Applied Physics, School of Physical and Mathematical Sciences, Nanyang Technological University, Singapore 637371, Singapore

[b] Department of Electronic and Electrical Engineering, University College London, Torrington Place, London, WC1E 7JE, United Kingdom

ARTICLE INFO

Article history:
Received 16 September 2009
Received in revised form
12 January 2010
Accepted 28 January 2010
by P. Hawrylak
Available online 4 February 2010

Keywords:
A. Quantum dots
D. Transition
E. Finite element analysis

ABSTRACT

The interband optical transitions of InAs/$In_xGa_{1-x}As$ dots-in-a-well (DWELL) structure is investigated theoretically and compared with experiment. The electronic structure was obtained by solving a steady-state effective-mass Schrödinger equation in cylindrical co-ordinates taking into account the strain effects. Optical transition energies as well as envelope functions of both electron and hole are calculated, respectively. The simulated transition energies agree very well with the experimental results. Our investigation is significant not only for the understanding of the optical properties of this novel material system, but also for the guidance of optimal structure design and growth.

1. Introduction

Self-assembled InAs/GaAs quantum dots (QDs) formed by strained epitaxy have been an important subject of recent research due to their unique physical properties and potential applications [1]. Various methods, such as atomic layer epitaxy (ALE) [2], covering InAs QDs with InGaAs and/or AlAs cap layer [3,4], etc., have been tried to extend the emission wavelength of InAs/GaAs QDs to 1.3 μm and 1.55 μm for the realization of the low cost, high performance devices for optical fiber telecommunication [5]. However, those techniques result in a low dot density which provides a low effective gain and it is therefore more difficult to achieve lasing [4]. Recently, a method has been developed to grow the dots within an InGaAs quantum well (QW), i.e., to form a so-called quantum dots-in-a-well (DWELL) structure [6]. It has been confirmed that higher InAs QDs density and better carrier confinement ability can be achieved by this novel structure [7,8]. Subsequently, considerable efforts have been devoted to explore the growth of such a structure. Comparatively, only few reports have been made regarding the modeling of optical absorption between subbands of the DWELL structure. For example, intersubband optical absorptions of an InAs/InGaAs DWELL infrared photodetectors were calculated in the framework of effective-mass envelope function theory without considering strain [9]. In terms of interband transitions, a two-step strain analysis of a relatively simple InAs/GaAs QD system was carried out by finite element method (FEM) [10]. A more precise eight-band model has been employed for a single InAs/GaAs dot [11], but it is too costly for complicated structures such as DWELL. So far there has been no report on the interband optical transitions in InAs/InGaAs DWELL structures. The difficulty lies mainly on the complicated potential profile which involves a two-dimensional QW and a zero-dimensional QD simultaneously, and the complex strain-induced modification of both the conduction band and valance band.

In this paper, we present our first attempt of numerical approach for interband optical transitions of a practical InAs/InGaAs DWELL structure. Energy bands under strain resulted from the mismatch of lattice constants between different materials are considered and then the data are used to construct the potential profile for solving the effective-mass Schrödinger equation. The precisely calculated energy levels provide a quantitative comparison with the available experimental data, which is important for the future optical analysis and applications.

2. Model of DWELL structure

The model system adopted is based on a practical sample, which was grown in a VG Semicon V80H MBE system on GaAs substrates [8]. QDs were formed by 2.8 ML InAs grown upon a 2 nm $In_xGa_{1-x}As$ ($x = 0.15$) strained buffer layer, and then covered with a 6 nm $In_xGa_{1-x}As$ strain-reducing layer with the same In mole fraction in SBL. After the DWELL structure growth at 505 °C, the nanostructure was capped with 15 nm GaAs follow by a 120 s long growth interruption and further GaAs cap growth at 615 °C which was referred to as the high growth temperature strain layer. The detailed growth and characterization of this novel structure can be

* Corresponding author. Tel.: +65 65138083; fax: +65 67957981.
E-mail address: hdsun@ntu.edu.sg (H.D. Sun).

0038-1098/$ – see front matter © 2010 Elsevier Ltd. All rights reserved.
doi:10.1016/j.ssc.2010.01.042

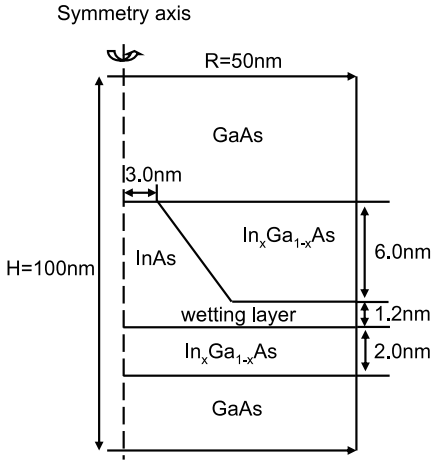

Fig. 1. Schematic of the InAs/InGaAs DWELL structure.

found elsewhere [12]. It has been shown that during the capping process, the original pyramidally shaped QDs became truncated [13]. From our previous cross-sectional transmission electron microscopy (TEM) [14] and scanning tunneling microscopy (STM) studies [15], a truncated pyramidal shape of QD nanostructures were also found, typical base lengths of 20–25 nm, and 5–7 nm height.

Using the information from the morphology study, the DWELL structure is defined and shown in Fig. 1. The model consists of a single truncated pyramidal InAs QD with dimension of 22 nm for the base and 6 nm for the height, which is placed between 2 nm and 6 nm InGaAs well and buried by GaAs. There is 2.8 ML (∼1.2 nm) [16] of InAs wetting layer (WL) between the first half of the quantum well and the quantum dot.

Numerical approach is formed by a cylinder of radius R and height H. We defined $R = 50$ nm and $H = 100$ nm which are big enough so that the envelope functions can be forced to vanish [17]. From atomic force microscopy (AFM) image [8], the dots density is estimated to be around 3.54×10^{10} cm^{-2}. Thus the average spacing between two adjacent dots is bigger than R. Hence, we ignore the coupling between the InAs QDs in this modeling.

2.1. Schrödinger equation in cylindrical co-ordinates

Energy levels of the quantum dot with WL assembly embedded in the $In_xGa_{1-x}As$ QW grown on the GaAs material can be obtained by solving the one-band steady-state Schrödinger equation:

$$-\frac{\hbar^2}{2}\nabla\cdot\left(\frac{1}{\mu(\vec{r})}\nabla\Psi(\vec{r})\right)+V(\vec{r})\Psi(\vec{r})=E\Psi(\vec{r}) \tag{1}$$

where $\hbar$ is Planck's constant divided by 2π, $\mu(\vec{r})$ is the space dependent electron or hole effective mass. $V(\vec{r})$ is the band edge potential energy dependent on the position vector $\vec{r}$, where we define $V(\vec{r})$ to be zero in InAs QD region, and $\Psi(\vec{r})$ is the envelope function. Due to cylindrical rotational symmetry is assumed, we have $\vec{r} = (\rho, z, \theta)$ where ρ is the axial co-ordinate, z is the radial co-ordinate and θ is the azimuthal angle in the range of 0–2π. Assuming that $\Psi(\vec{r})$ has a separable form in θ, then $\Psi = \Psi_1(\rho, z)\Psi_2(\theta)$ and Eq. (1) becomes,

$$-\frac{\hbar^2}{2\mu}\left[\frac{1}{\rho}\frac{\partial}{\partial\rho}\left(\rho\frac{\partial\Psi_1}{\partial\rho}\right)+\frac{\partial^2\Psi_1}{\partial z^2}\right]\Psi_2+(V-E)\Psi_1\Psi_2 = \frac{\hbar^2}{2\mu}\frac{1}{\rho^2}\frac{\partial^2\Psi_2}{\partial\theta^2}\Psi_1. \tag{2}$$

Dividing Eq. (2) with $\frac{\Psi_1\Psi_2}{\mu\rho^2}$ and rearranging the terms lead to

$$-\frac{\hbar^2}{2}\frac{\rho^2}{\Psi_1}\left[\frac{1}{\rho}\frac{\partial}{\partial\rho}\left(\rho\frac{\partial\Psi_1}{\partial\rho}\right)+\frac{\partial^2\Psi_1}{\partial z^2}\right]+\mu\rho^2(V-E) = \frac{\hbar^2}{2}\frac{1}{\Psi_2}\frac{\partial^2\Psi_2}{\partial\theta^2}. \tag{3}$$

Since each side of this equation is independent of each other, the last expression of $\Psi_2(\theta)$ can be solved to give $\Psi_2(\theta) = \exp(im_l\theta)$ and the remaining part can be written as,

$$-\frac{\hbar^2}{2\mu}\left[\frac{\partial^2\Psi_1}{\partial\rho^2}+\frac{\partial^2\Psi_1}{\partial z^2}\right]-\frac{\hbar^2}{2\mu\rho}\frac{\partial\Psi_1}{\partial\rho}+\left(\frac{\hbar^2 m_l^2}{2\mu\rho^2}+V\right)\Psi_1 = E\Psi_1. \tag{4}$$

The envelope function can be written as: $\Psi = \Psi_1(\rho, z)\exp(im_l\theta)$, where m_l must be an integer to hold the boundary condition $\Psi_2(0) = \Psi_2(2\pi)$. For the symmetrical axis, special treatment should be performed. When m_l is non-zero, Dirichlet boundary conditions ($\Psi_1 = 0$) must be imposed at this symmetry line; However, when $m_l = 0$, this term changes to Neumann boundary conditions ($\frac{\partial\Psi_1}{\partial\rho} = 0$).

2.2. Energy bands under strain

For solving effective-mass Schrödinger Eq. (4), potential energy $V(\vec{r})$ of different layers must be known. Hence, energy bands calculation of different materials under strain will be presented.

Because of lattice constant mismatch between different materials, hydrostatic and uniaxial strains will be induced. Hydrostatic strain will influence the lattice volume resulting in energy level change of materials, while uniaxial strain will destroy symmetry which leads to valence band degeneracy. Van de Walle [18] has done detailed calculation of the influence of energy band by strain. The initial normal strains in the x-, y-and z-directions can be defined as:

$$\varepsilon_{xx} = \varepsilon_{yy} = \frac{a_1 - a_2}{a_2}, \qquad \varepsilon_{zz} = -2\frac{C_{12}}{C_{11}}\varepsilon_{xx} \tag{5}$$

where a_1 and a_2 are the lattice constants of the substrate and deposited material respectively. C_{11} and C_{12} are the components of the two-order tensor of elastic moduli. The change of the volume is related to the stress tensor, which is

$$\frac{\Delta\Omega}{\Omega} = Tr(\vec{\varepsilon}) = (\varepsilon_{xx}+\varepsilon_{yy}+\varepsilon_{zz}) \tag{6}$$

and the energy of conduction band and valence band also changed with the this component,

$$\Delta E_C = a_C\frac{\Delta\Omega}{\Omega} \quad \text{and} \quad \Delta E_{V,aV} = a_V\frac{\Delta\Omega}{\Omega} \tag{7}$$

where a_C and a_V are hydrostatic deformation potential of conduction band and valence band respectively. For uniaxial strain, the change of energy band of heavy hole is

$$\Delta E_{HH} = \frac{1}{3}\Delta_0 - \frac{1}{2}\delta E_{00} \tag{8}$$

where $\delta E_{001} = 2b(\varepsilon_{zz} - \varepsilon_{xx})$ and b is the shear deformation potential of the material. Thus the energy band of a material with strain is expressed as

$$E_g = E_{g0} + \Delta E_C - \Delta E_V - \Delta E_{HH} \tag{9}$$

where E_{g0} is the initial energy band of materials without strain. By using Eq. (9) energy bands of $In_xGa_{1-x}As$/GaAs and InAs/$In_xGa_{1-x}As$ materials can be obtained. For doing this kind of calculation, parameters should be carefully chosen [19]. Some alloy parameters of $In_xGa_{1-x}As$ are interpolated from the values of InAs and GaAs. They are listed in Table 1.

Table 1
Material parameters for $In_xGa_{1-x}As$ as a function of the In mole fraction x.

E_{g0} (eV)[a]	$a_C(x)$ (eV)[b]	$a_V(x)$ (eV)[b]	Δ_0 (eV)[b]
$1.508 - 1.470x + 0.375x^2$ (77 K) $1.425 - 1.501x + 0.436x^2$ (300 K)	$-8.0113 + 2.933x$	$0.22 + 0.781x$	$0.34-0.0993x+0.133x^2$
μ (m_0)[c]	$C_{11}(x)$ (10^{11}Pa)[b]	$C_{12}(x)$ (10^{11}Pa)[b]	$b(x)$ (eV)[b]
$\mu_e = 0.063 - 0.043x + 0.003x^2$ $\mu_h = 0.51 - 0.1x$	$1.188 - 0.355x^2$	$0.538 - 0.085x^2$	$-1.824 + 0.024x$

[a] Reference [21].
[b] Reference [11].
[c] Reference [22].

Table 2
Comparison of simulated result with experiment data.

Temperature (K)	Strain consideration	Energy level (eV)		Experimental value (eV)		Calculated value (eV)	
		InGaAs	InAs	E_0	E_1	E_0	E_1
77	Without	1.2960	0.4130	0.999	1.052	0.639	0.686
	With	1.3150	0.8151			0.997	1.041
300	Without	1.2096	0.3600	0.935	0.979	0.582	0.630
	With	1.2287	0.7621			0.939	0.983

Aforementioned results were treated as the initial potential profiles of different layers for the calculation of Schrödinger equation. The conduction band offset between the strained InAs/GaAs and $In_xGa_{1-x}As$/GaAs is taken to be 60% of their difference in band gaps [20]. Eq. (4) can be numerically solved by means of a FEM package COMSOL Multiphysics using the partial differential equation (PDE) modes. Conduction and valence bands have been treated separately, and then quantum confinement energies and envelope functions for electron and hole can be obtained by solving Eq. (4).

The optical transitions from InAs/InGaAs DWELL structure can be expressed as

$$E = E_{g\mathrm{InAs}} + E_{eigC} + E_{eig} \tag{10}$$

where $E_{g\mathrm{InAs}}$ is the InAs energy band under strain, E_{eigC} and E_{eigV} are the confinement energy of electron and hole, respectively.

3. Results and discussion

Experimental measurements of Photoluminescence (PL) were performed with a He–Cd laser emitting at 442 nm as the excitation source. The PL emission was detected using a Peltier cooled InGaAs photodiode and measured by standard lock-in amplifier technique. Fig. 2 illustrates the PL spectra of the InAs/InGaAs DWELL structure measured at 77 and 300 K, respectively. The closed squares and open circles represent the interband transitions of ground state (GS) and the first excited state (FES), respectively, which is verified by excitation intensity dependent PL spectra. Table 2 shows the comparison between the experimental values and the optical transition energies for GS and FES obtained using our model. It reveals that without considering strain effect, the model gives too low energy levels at the two different temperatures unless parameters are changed to physically unrealistic values. In contrast, when considering strain effect, the calculated GS and FES transition energies agree very well with the experimental PL data, which indicated the importance of strain effect in the QD simulation of optical transitions.

Next, envelope functions of InAs/InGaAs DWELL structure were examined. Figs. 3(a)–(b) are the electron and hole probability envelope functions for the GS of this particular QD. The figures reveal that GS envelope functions are confined well in the QD region, which have an atomic-orbital-like s-type. There are slightly differences between electron and hole due to their different properties such as confinement potentials and effective masses. In contrast to GS, electron envelope function of FES [Fig. 3(c)] moves to the joint

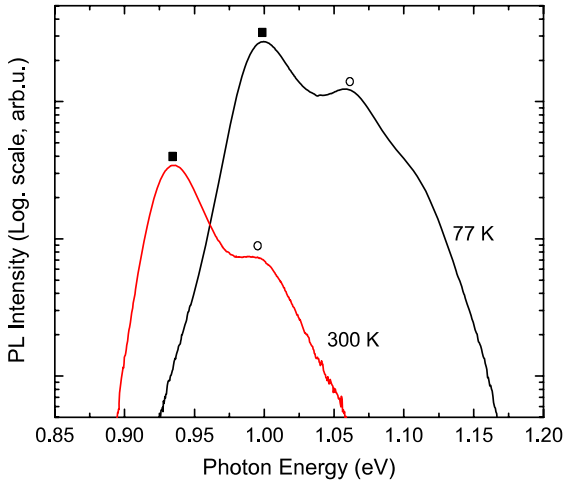

Fig. 2. (Color online) PL spectra of InAs/InGaAs DWELL structures. Square and circle indicated ground state and the first excited state, respectively.

of QD region and WL, indicating the trend of coupling between QD and WL region, although the coupling is relatively weak. This phenomenon is more obvious for a higher excited state [Fig. 3(d)]. It shows that this higher excited state has a stronger presence close to the QD region. Such states are expected to play an important role in carrier capture from WL to QD [23,24]. Similar results have been reported in Ref. [25,26].

Different samples with different In mole fraction in the $In_xGa_{1-x}As$ QW have also been tried. However, because of the lack of information about the dimension of the specific QDs, the simulated results are not comparable. Nevertheless, the proposed methodology in this paper can be readily extended for other geometric configurations.

4. Conclusions

In this paper, a numerical approach for calculating the interband optical transition of an InAs/InGaAs DWELL structure is presented. Energy levels of different materials under strain effects are analyzed in detail, and the energy levels are treated as initial potential profiles for calculating the one-band Schrödinger equation under cylinder symmetry in the framework of effective-mass envelope function theory with the aid of COMSOL Multiphysics. The

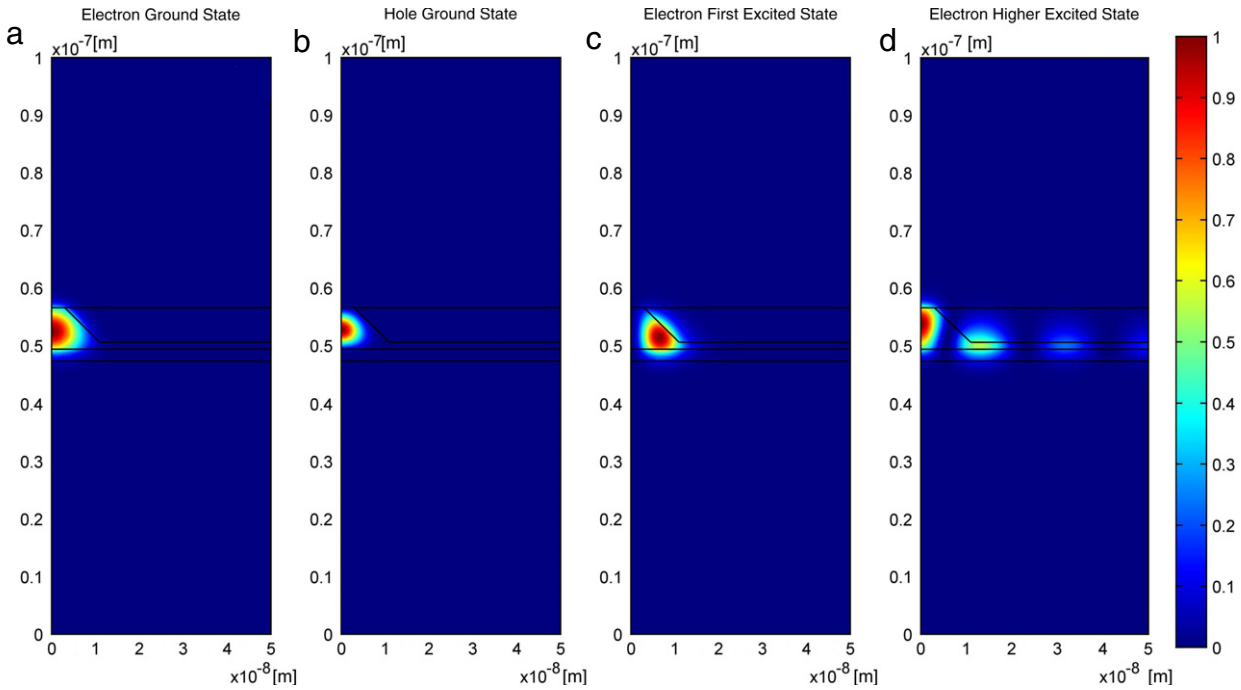

Fig. 3. (Color online) Envelope functions of InAs/$In_xGa_{1-x}As$ ($x = 0.15$) DWELL structure. (a) Electron ground state, (b) hole ground state, (c) electron first excited state, (d) electron higher excited state.

combined exploration of theoretical calculation and experimental measurement is crucial for the better understanding of the physical properties of InAs self-assembled QDs grown inside quantum well structures, and is of great significance in QD material design and fabrication.

References

[1] H.Y. Liu, B. Xu, Y.Q. Wei, D. Ding, J.J. Qian, Q. Han, J.B. Liang, Z.G. Wang, Appl. Phys. Lett. 79 (2001) 2868.
[2] D.L. Huffaker, D.G. Deppe, Appl. Phys. Lett. 73 (1998) 520.
[3] M. Arzberger, U. Kasberger, G. Bohm, G. Abstreiter, Appl. Phys. Lett. 75 (1999) 3968.
[4] N. Kenichi, S. Hideaki, S. Shigeo, L. Jeong-Sik, Appl. Phys. Lett. 74 (1999) 1111.
[5] V.M. Ustinov, A.E. Zhukov, Semicond. Sci. Technol. 15 (2000) R41.
[6] V.M. Ustinov, N.A. Maleev, A.E. Zhukov, A.R. Kovsh, A.Y. Egorov, A.V. Lunev, B.V. Volovik, I.L. Krestnikov, G.M. Yu, N.A. Bert, P.S. Kop'ev, I.A. Zh, N.N. Ledentsov, D. Bimberg, Appl. Phys. Lett. 74 (1999) 2815.
[7] J.X. Chen, U. Oesterle, A. Fiore, R.P. Stanley, M. Ilegems, T. Todaro, Appl. Phys. Lett. 79 (2001) 3681.
[8] H.Y. Liu, M. Hopkinson, C.N. Harrison, M.J. Steer, R. Frith, I.R. Sellers, D.J. Mowbray, M.S. Skolnick, J. Appl. Phys. 93 (2003) 2931.
[9] X.X. Han, J.M. Li, J.J. Wu, G.W. Cong, X.G. Liu, Q.S. Zhu, Z.G. Wang, J. Appl. Phys. 98 (2005) 053703.
[10] M.K. Kuo, T.R. Lin, K.B. Hong, B.T. Liao, H.T. Lee, C.H. Yu, Semicond. Sci. Technol. 21 (2006) 626.
[11] O. Stier, M. Grundmann, D. Bimberg, Phys. Rev. B 59 (1999) 5688.
[12] H.Y. Liu, I.R. Sellers, T.J. Badcock, D.J. Mowbray, M.S. Skolnick, K.M. Groom, M. Gutierrez, M. Hopkinson, J.S. Ng, J.P.R. David, R. Beanland, Appl. Phys. Lett. 85 (2004) 704.
[13] H. Eisele, A. Lenz, R. Heitz, R. Timm, M. Dahne, Y. Temko, T. Suzuki, K. Jacobi, J. Appl. Phys. 104 (2008) 124301.
[14] H.Y. Liu, C.M. Tey, I.R. Sellers, T.J. Badcock, D.J. Mowbray, M.S. Skolnick, R. Beanland, M. Hopkinson, A.G. Cullis, J. Appl. Phys. 98 (2005) 083516.
[15] A. Lenz, H. Eisele, R. Timm, L. Ivanova, H.Y. Liu, M. Hopkinson, U.W. Pohl, M. Dähnea, Physica E: Low-Dimensional Systems and Nanostructures 40 (2008) 1988.
[16] M.A. Naser, M.J. Deen, D.A. Thompson, J. Appl. Phys. 100 (2006) 093102.
[17] A. Amtout, S. Raghavan, P. Rotella, G.v. Winckel, A. Stintz, S. Krishna, J. Appl. Phys. 96 (2004) 3782.
[18] C.G. Van de Walle, Phys. Rev. B 39 (1989) 1871.
[19] A.P. Zhou, W.D. Sheng, Eur. Phys. J. B 68 (2009) 233.
[20] S.K. Emil, J. Appl. Phys. 73 (1993) 8480.
[21] G. Ji, D. Huang, U.K. Reddy, T.S. Henderson, R. Houdre, H. Morkoc, J. Appl. Phys. 62 (1987) 3366.
[22] Y.A. Goldberg, N.M. Schmidt, in: M. Levinshtein, S. Rumyantsev, M. Shur (Eds.), Handbook Series on Semiconductor Parameters, World Scientific, London, 1999, p. 62.
[23] S. Raymond, K. Hinzer, S. Fafard, J.L. Merz, Phys. Rev. B 61 (2000) R16331.
[24] R. Chen, H.Y. Liu, H.D. Sun, J. Appl. Phys. 107 (2010) 013513.
[25] M.M. Betcke, H. Voss, Nanotechnology 19 (2008) 165204.
[26] R.V.N. Melnik, M. Willatzen, Nanotechnology 51 (2004) 1.